Biophysical Journal Volume 103 July 2012 19–28

Normal-Mode-Analysis-Guided Investigation of Crucial Intersubunit Contacts in the cAMP-Dependent Gating in HCN Channels

Farzana Marni,[△] Shengjun Wu,[△] Gaurav M. Shah, Xin-ping Xu, Amber R. Hackett, Changan Xie, Sabisha Shrestha, Lin Liu, Qinglian Liu, and Lei Zhou*
Department of Physiology and Biophysics, School of Medicine, Virginia Commonwealth University, Richmond, Virginia

ABSTRACT Protein structures define a complex network of atomic interactions in three dimensions. Direct visualization of the structure and analysis of the interaction potential energy are not straightforward approaches to pinpoint the atomic contacts that are crucial for protein function. We used the tetrameric hyperpolarization-activated cAMP-regulated (HCN) channel as a model system to study the intersubunit contacts in cAMP-dependent gating. To obtain a systematic survey of the contacts between each pair of residues, we used normal-mode analysis, a computational approach for studying protein dynamics, and constructed the covariance matrix for C-α atoms. The significant contacts revealed by covariance analysis were further investigated by means of mutagenesis and functional assays. Among the mutant channels that show phenotypes different from those of the wild-type, we focused on two mutant channels that express opposite changes in cAMP-dependent gating. Subsequent biochemical assays on isolated C-terminal fragments, including the cAMP binding domain, revealed only minimal effects on cAMP binding, suggesting the necessity of interpreting the cAMP-dependent allosteric regulation at the whole-channel level. For this purpose, we applied the patch-clamp fluorometry technique and observed correlated changes in the dynamic, state-dependent cAMP binding in the mutant channels. This study not only provides further understanding of the intersubunit contacts in allosteric coupling in the HCN channel, it also illustrates an effective strategy for delineating important atomic contacts within a structure.

INTRODUCTION

Ion channels are an excellent research target for the study of protein allostery because their activities in response to membrane potential changes or chemical cues can be faithfully recorded by electrophysiological methods (1–3). During the past decade, structural biology techniques, especially x-ray crystallography, have been widely used in the field of ion channel biophysics, and have provided exciting insights at the atomic level. An experimentally determined protein structure represents the conformation corresponding to a local minimum on the energy surface, and can be used as a solid platform for launching further computational and functional studies. Starting from a newly solved crystal structure, a common practice is to design site-directed mutagenesis and then test the predictions by using functional assays. However, pinpointing the crucial atomic contacts among the network of contacts contained within the structure is not a trivial task. Delineating which contacts are important for allosteric coupling is especially challenging, because in general allosteric contacts are located at a distance away from the structural domains that sense the stimuli (e.g., the ligand- and substrate-binding sites) or the functional domains (e.g., the ion-conducting pore and the catalytic site in a protein enzyme). Hence, it has been difficult to determine the structural basis underlying allosteric coupling.

In this study, we aimed to investigate allosteric contacts from the standpoint of protein dynamics, which is increasingly being recognized to contain important information for protein function. Studies on protein enzymes have revealed an intriguing connection between enzyme catalytic activity and collective molecular motions, which involve every structural element in the system and describe a concerted action among them (4–8). The collective motions of the lowest vibration frequencies and the largest amplitudes dominate the atomic fluctuations and are the most functionally relevant (9–12). Investigators have developed several computational approaches to study protein dynamics, including normal-mode analysis (NMA), an analytical approach based on a harmonic approximation to protein energy surface, and principal component analysis (PCA, also called essential dynamics), a statistical approach that is applied to an ensemble of protein conformations collected in molecular-dynamics (MD) or Monte Carlo (MC) simulations (13–15). Both approaches employ analysis of covariance or cross-correlation of atomic positional fluctuations (16). To identify the crucial contacts, we used NMA to extract the directionality (eigenvector) and the frequency (eigenvalue) of the collective motions. The eigenvectors of the lowest vibration frequencies were used to construct an essential covariance matrix for C-α atoms, which represents a systematic and quantitative survey of all contacts between each pair of residues (16).

In this study, we chose to use the hyperpolarization-activated cAMP-regulated (HCN) channel as our research target, and investigated the role of intersubunit contacts

Submitted December 22, 2011, and accepted for publication May 22, 2012.
[△]Farzana Marni and Shengjun Wu contributed equally to this work.
*Correspondence: lzhou@vcu.edu
S. Shrestha's present address is Virginia Blood Services, Richmond, VA.
Editor: Jose Faraldo-Gomez.

0006-3495/12/07/0019/10 $2.00
doi: 10.1016/j.bpj.2012.05.030

in cAMP-dependent allosteric regulation. Unlike other voltage-gated channels, HCN channels open upon membrane hyperpolarization (17,18). On the intracellular side, the HCN channel carries a canonical cyclic nucleotide-binding domain (CNBD). Direct cAMP binding facilitates the activity of the HCN channel by shifting the voltage dependence toward less negative potentials and increasing the macroscopic current amplitude. Each HCN channel contains four subunits. Within each subunit, there is a transmembrane domain (TMD) homologous to that of voltage-gated K^+ channels, a CNBD in the C-terminus, and a C-linker (CL) in between (19–22). The CL-CNBD fragment functions as the essential molecular machinery for cAMP-dependent gating. Structures of the CL-CNBD domain from the mouse HCN2 (mHCN2) and the human HCN4 channel have been determined by x-ray crystallography (23,24). These structures provide a detailed view of the local contacts between cAMP and CNBD, as well as the subunit assembly. However, all of these structures share an identical folding scheme with the root mean-square deviation (RMSD) of the C-α atoms < 1 Å. It remains unclear how cAMP binding to the CNBD triggers a series of local and global structural rearrangements to allosterically affect the movement of the gate, which is located ~50 Å away in the TMD.

Numerous biophysical studies support a rather complicated cooperativity among the four subunits during cAMP-dependent gating in the HCN channel (25–27). CL-CNBD structures reveal an extensive network of interactions between neighboring subunits, especially in the CL region; however, the roles of these interactions in allosteric coupling remain to be clarified. At the whole-channel protein level, previous studies on HCN or related cyclic nucleotide-gated (CNG) channels revealed the contributions of the N-terminal fragment, the pore, and residues to the CL, but a comprehensive understanding of the contributions of intersubunit contacts has been lacking (28–31). Here, based on the CL-CNBD crystal structure, we applied NMA-based covariance analysis to identify critical contacts. Promising candidates were further tested by mutagenesis experiments. To elucidate the molecular mechanism, we applied a multidisciplinary approach that was critical to gain an understanding from complementary angles.

RESULTS

NMA-based covariance analysis is effective for systematically surveying atomic contacts

The HCN CL-CNBD structure shows an extensive network of intersubunit interactions within the tetrameric assembly of four fragments (Fig. 1, *A* and *B*) (23). To better reproduce the protein's dynamic behavior in its native environment, a 5 Å layer of water molecules was maintained on the protein's surface during the NMA based on an all-atoms representation (AANMA) (Supporting Material) (32,33). The first 100 eigenvectors of the lowest vibration frequencies were used to calculate the covariance matrix. To illustrate portions of the covariance matrix for intra- and intersubunit contacts, we chose to use subunit B as an example, with intrasubunit contacts shown in the middle and intersubunit contacts with the neighboring subunit A (*left*) or subunit C (*right*) shown on each side (Fig. 1 *C*). An examination of the panels marked B-A and B-C reveals three clusters of contacts (indicated by *blue circles*). These potentially significant contacts are located at the interfaces between CL-CL, CL-CNBD, and CNBD-CNBD from neighboring subunits and symmetrically distributed at the A-B and B-C interfaces.

The above analysis is based on an all-atoms representation in which all atoms, including those of surface water molecules, are treated explicitly. This representation incorporates contributions from chemical details embedded in side chains and bound cAMP molecules. To confirm the robustness and accuracy of this approach, we used a coarse-grained NMA based on the anisotropic network model (ANM), which is based on a simple representation of the system in which only C-α atoms are considered with the unified force constant set as 1 kcal/mol/Å^2 (34,35). Impressively, this minimalist treatment effectively captures the essentials of the energy, structure, and dynamics, and reproduced experimental observations not only for the protein but also for DNA and RNA systems (36). Using the same set of C-α atoms from the above AANMA, we carried out an ANM analysis and used the first five out of a total of 2394 eigenvectors to construct the covariance matrix (Fig. 1 *D* and Fig. S1 in the Supporting Material). The ANM results match the AANMA results and yield the same three intersubunit contact clusters.

To validate this strategy for NMA-covariance analysis, we examined the contacts between cAMP and residues of CNBD, which had been extensively studied by experimental approaches. We started from an AANMA that incorporated more detailed chemical information and constructed a covariance matrix for all cAMP atoms and C-α atoms (Fig. 2 *A*). The covariance analysis revealed that residues in close contact with cAMP include R591, T592, and R632, among others. Indeed, most of these residues were confirmed by previous experimental studies to be crucial for ligand binding (22,28,37). To further validate this covariance analysis approach, we analyzed the contacts within a single subunit and ascertained whether basic structural features, such as the secondary structures, could be captured (Fig. 2 *B*). Because all atoms, including those of protein and water molecules, are treated nondiscriminatively during AANMA, the ability to reproduce the secondary structures, which are not part of the input to the simulation system, can be used as a criterion to measure the effectiveness of this method. As illustrated in Fig. 2 *B*, the pattern of stable contacts matches well with the definition of secondary structures in the original crystal structure. Thus, our analyses of cAMP-protein contacts and intrasubunit contacts convince

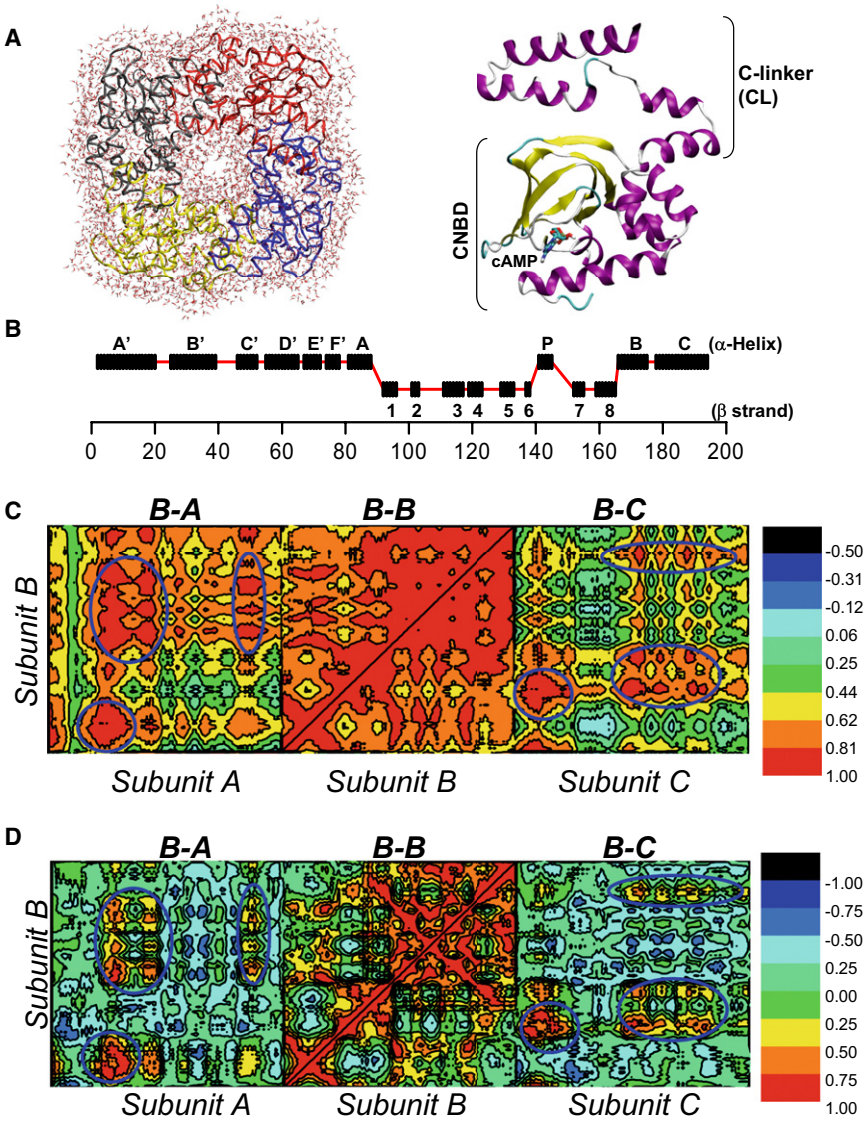

FIGURE 1 NMA-based covariance analysis of the tetrameric CL-CNBD assembly in HCN channels. (*A*) Left: View of the CL-CNBD structure covered with a 5 Å layer of surface water molecules. Right: Side view of a single subunit. (*B*) Secondary structures within a single subunit. CL includes six α-helixes (A′–F′), and CNBD includes four α-helixes (A, P, B, and C) and eight β-strands (β1–β8). (*C*) Covariance matrix of C-α atoms based on AANMA. To simplify the illustration, one representative subunit (subunit B) and two neighboring subunits (subunits A and C) are shown. (*D*) Covariance matrix of C-α atoms based on ANM.

us that the covariance analysis based on NMA is able to provide reliable and useful information for delineating significant atomic contacts.

Experimental tests of predicted interfacial contacts between neighboring subunits

On the basis of the above computational analysis, we examined the corresponding primary sequence and identified the residues that potentially support those intersubunit contacts (Fig. 2 *C*). We started with charged residues and screened each one by alanine replacement. We then characterized the mutant channels by using three complementary approaches: two-electrode voltage-clamp (TEVC) recording in the whole-cell configuration, patch-clamp recording of channel activities from excised membrane patch, and patch-clamp fluorometry (PCF) recording of cAMP binding together with channel activities (Supporting Material). TEVC traces in response to a series of hyperpolarizing voltage steps are shown in Fig. 3 *A*. The amplitude of the tail current measured at −40 mV reflects the extent of channel activation by each voltage step. The Boltzmann equation was used to fit the instantaneous amplitudes of the tail currents plotted as a function of voltage. $V_{1/2}$ corresponds to the voltage step that generates half of the maximum activation. Of note, due to slow activation of the mHCN2 channel, the $V_{1/2}$-value we obtained with 3-s voltage steps is more negative than that previously obtained under a fully equilibrated, steady-state condition (38,39).

Because the $K_{1/2}$ (EC_{50}) for cAMP to regulate the voltage gating of the wild-type (WT) mHCN2 channel is ~0.1 μM, and the intracellular cAMP concentration in an intact oocyte is in the micromolar range, TEVC traces of WT channel actually reflect the channel's behavior under a saturating concentration of cAMP (40). Therefore, we used the mutant channel mHCN2/R591E as a negative control for measuring

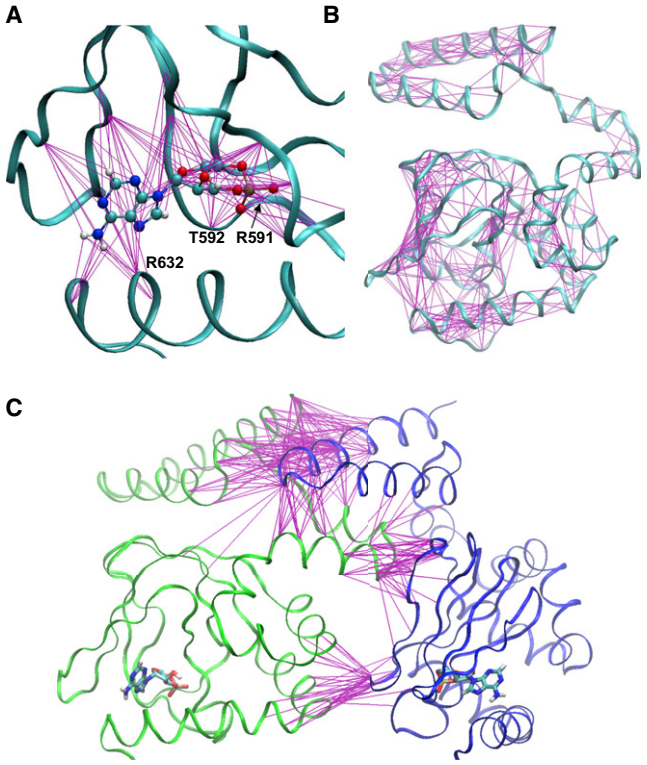

FIGURE 2 Significant cAMP-CNBD contacts (intra- and intersubunit) identified by AANMA-based covariance analysis. (*A*) Significant contacts between cAMP and protein residues from CNBD. Each line links a pair of atoms from the cAMP molecule and C-α atoms with a covariance factor of >0.97. Most of the residues identified here (e.g., R591, T592, and R632) have been confirmed to be critical by experiments (37). (*B*) Significant intrasubunit contacts successfully replicate elements of secondary structures. Each line represents a pair of C-α atoms with a covariance factor of >0.90. Only the residue pairs that were more than three residues apart are considered. (*C*) Significant intersubunit contacts revealed by covariance analysis. Each line represents a pair of residues with a covariance factor of >0.90.

the response to cAMP. The location of R591 is highly conserved among not only HCN but also CNG channels and protein kinases. The R591E mutation largely abolishes cAMP binding but leaves no effect on the efficacy of cAMP regulation, as indicated by maximal $\Delta V_{1/2}$ (24,41). Compared with the WT channel, R591E mutation makes the channel activate more slowly and deactivate more rapidly (Fig. 3 *A*, *top*). Moreover, the $V_{1/2}$ is −10.7 mV more negative. All of these differences between WT and R591E channels reflect the contribution from cAMP-dependent gating.

Next, we employed TEVC recording to screen the mutant channels. Most of the channels showed significant changes in the $V_{1/2}$ and the time constant for activation or deactivation (Table S1). We focused on two mutant channels, K452A and R590A, which express opposite changes in channel kinetics and $V_{1/2}$ (Fig. 3 *A*, *bottom*, and Fig. S3). The $V_{1/2}$ of mHCN2/K452A is comparable to that of the WT channel but opens much faster and deactivates more slowly, which indicates a possible enhanced response to cAMP. In contrast, the $V_{1/2}$ of R590A is −11.3 mV more negative than that of the WT channel and close to that of R591E. Moreover, the R590A channel opens slowly and deactivates much faster, consistent with a diminished response to cAMP (Fig. 3 *B*).

To quantify the changes in the cAMP-dependent gating, we employed patch-clamp recording on an excised membrane patch in the inside-out configuration. By applying different concentrations of cAMP to the bath and measuring the corresponding $\Delta V_{1/2}$, we derived the values of $K_{1/2}$ (EC_{50}) and the maximal $\Delta V_{1/2}$ from the dose-response curve Similarly to the TEVC results, the patch-clamp recordings for K452A revealed a slight decrease in $K_{1/2}$ (WT: 0.09 ± 0.01 μM; K452A: 0.05 ± 0.01 μM) and, impressively, a 30% increase in the maximal $\Delta V_{1/2}$ (WT: 16.8 ± 0.4 mV; K452A: 23.72 ± 1.2 mV). Both measurements clearly demonstrate an enhanced response to cAMP in K452A channel. In contrast, in the R590A channel, the sensitivity to cAMP was significantly reduced as measured by $K_{1/2}$ (0.87 ± 0.24 μM). The maximal $\Delta V_{1/2}$ was reduced to ~59% of the WT value (10.2 ± 0.6 mV; Fig. 3 *D*). Both measurements suggest that R590A negatively affects cAMP-dependent gating. However, the contribution of R590 is intrinsically different from that of R591, because the R591A mutation reduces the sensitivity to cAMP by ~30-fold but has no effect on the maximal $V_{1/2}$ (37). Altogether, the patch-clamp recordings provide strong evidence that both K452A and R590A mutations affect the cAMP-dependent regulation of channel activity. Because both residues are located at a distance away from the core of CNBD and mediate intersubunit contacts, they should contribute more to allosteric coupling than to cAMP binding.

Minimal effects on local cAMP-CNBD interactions by K452A and R590A

To determine whether these mutations affect local cAMP-CNBD interactions, we purified the CL-CNBD fragment and measured the binding affinity (Kd) using isothermal titration calorimetry (ITC) and fluorescence anisotropy (FA) methods (Fig. 4 and Supporting Material). For WT mHCN2 protein, the measured Kd is in the micromolar range (ITC: 2.47 ± 0.30 μM, $n = 9$; FA: 0.32 ± 0.04 μM, $n = 3$). The quantitative difference between the results may be due to the different physics underlying ITC and FA. The K452A sample did not show any significant changes in Kd (ITC: 2.14 ± 0.19 μM, $n = 3$; FA: 0.41 ± 0.18 μM, $n = 3$) or heat release upon cAMP binding (ΔH; Fig. 4 *C*). In the R590A mutant protein, there was a slight decrease in the binding affinity (ITC: 6.84 ± 0.74 μM, $n = 3$; FA: 0.52 ± 0.31 μM, $n = 3$) but no apparent change in the heat release (ΔH). Of note, this reduction in Kd is moderate and should not account for the ninefold increase in EC_{50} or the 40% decrease in maximal $V_{1/2}$ observed in the full-length R590A channel. Clearly, these biochemical assays provide useful information about the binding of

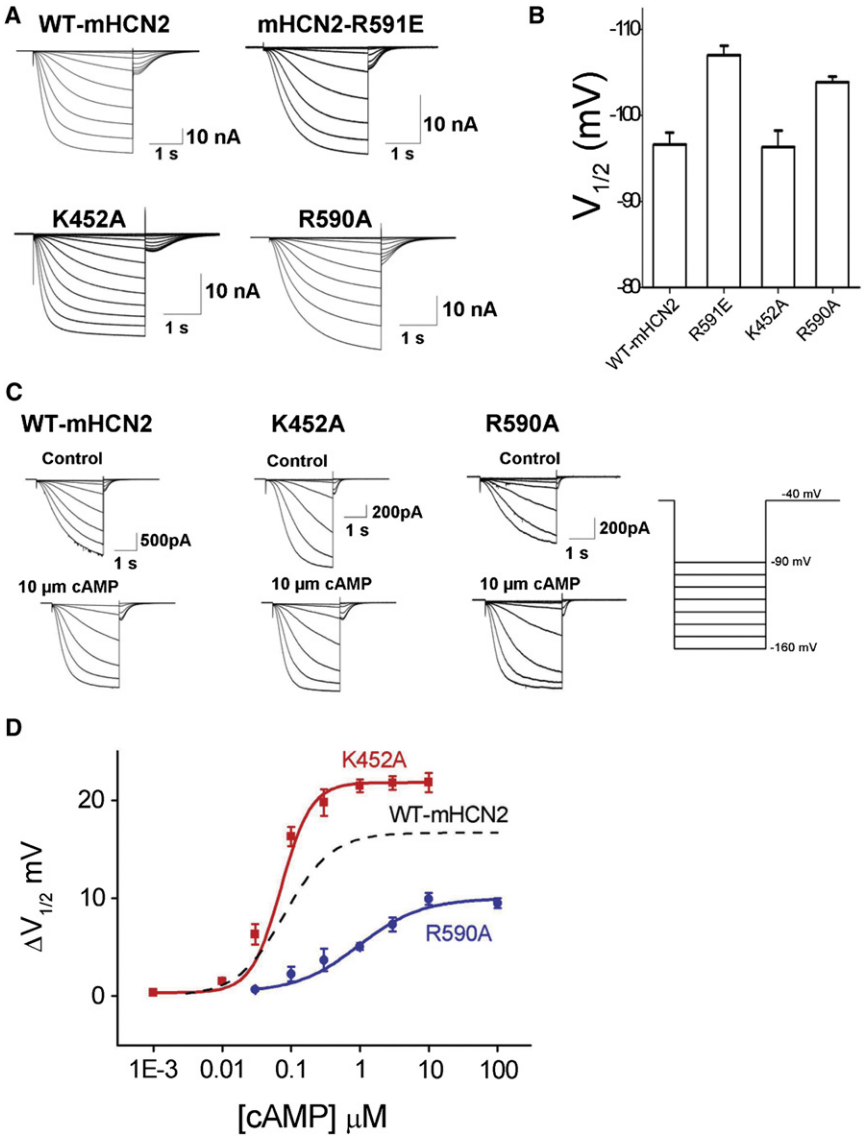

FIGURE 3 TEVC and patch-clamp recordings of two representative mutant channels: K452A and R590A. (*A*) Raw TEVC recording traces. Top: WT mHCN2 (*left*) and R591E mutant channels (*right*) were used as positive and negative controls, respectively, for cAMP binding. Bottom: K452A (*left*) and R590A (*right*) mutant channels. (*B*) $V_{1/2}$-values based on TEVC recordings. An independent *t*-test shows that R591E and R590A channels are significantly different from the WT channel ($p < 0.001$). (*C*) Patch-clamp recordings of HCN channels in the inside-out configuration. Left: WT. Middle: K452A. Right: R590A. Top: Control without cAMP. Bottom: 10 μM cAMP in the bath. The voltage protocol is shown on the right. (*D*) Dose-response curve showing the shift in voltage gating ($\Delta V_{1/2}$) versus cAMP concentration. At 10 μM, an independent-samples *t*-test showed that both mutant channels were significantly different from the WT channel (K452A, $t = 4.15$, $p < 0.005$; R590A, $t = 7.17$, $t < 0.001$).

cAMP to isolated CL-CNDB fragments, but limited information about changes in the gating of full-length channels, reinforcing the idea that both mutations affect the allosteric coupling mediated by intersubunit contacts instead of local contacts between cAMP and CNBD. From another angle, these results highlight the importance of interpreting ligand gating at the whole-channel level.

We also conducted an MD simulation to study how the WT CL-CNBD structure, the starting point for the MD simulations, evolves upon introduction of the K452A or R590A mutation. Our major focus was the structural perturbations localized to the point mutations, rather than global changes such as the subunit assembly. We monitored the distances of K452-E494 and R590-E617, two pairs of oppositely charged residues in close proximity (Fig. 5, *A* and *B*). For the WT protein, the sharp peaks in the histograms reflect very stable interfacial contacts (Fig. 5, *C–F*). In contrast, upon the introduction of both mutations, we observed time-dependent drifts in both distances. It is clear that near the end of the 20-ns simulation, two stable contacts observed in the WT simulations were destabilized. Structural change at the global level is an interesting direction to pursue, but currently such an investigation would be challenging in standard MD simulations (43–45). Nevertheless, our MD simulation results indicate that electrostatic interactions involving either K452 or R590 play an important role in stabilizing the contacts between neighboring subunits.

Interfacial mutations affect state-dependent interactions between cAMP and the full-length channel

An assay addressing the global interactions between cAMP and the full-length channel should be able to provide insight

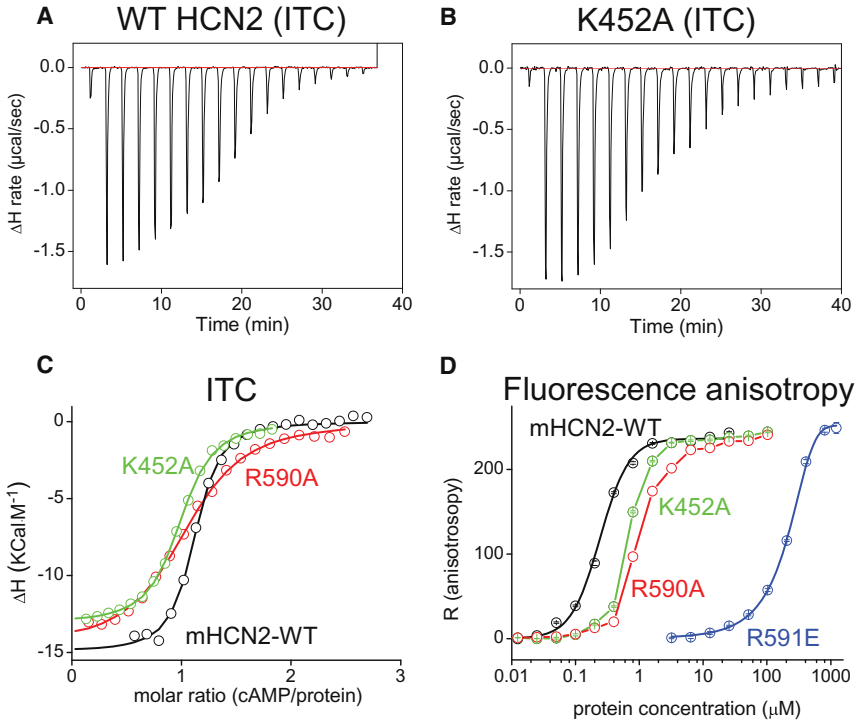

FIGURE 4 K452A and R590A mutations have minimal effects on the binding of cAMP to an isolated CL-CNBD domain. (*A*) Raw ITC results for WT protein. The rate of heat change is plotted as a function of cAMP injection time. (*B*) ITC results for K452A protein. (*C*) ITC traces showing heat change versus the molar ratio of cAMP to protein. The measured Kd values were 2.47 ± 0.30 μM ($n = 9$) for WT protein, 2.14 ± 0.19 μM ($n = 3$) for K452A, and 6.84 ± 0.74 μM ($n = 3$) for R590A. The R590A result is significantly different from that of the WT sample ($p < 0.05$). ITC is not sensitive for low-affinity binding such as that observed for R591E. (*D*) FA results showing the binding of 8-Fluo-cAMP to WT, K452A, R590, and R591E proteins. The measured Kd values were 0.32 ± 0.04 μM ($n = 3$) for WT mHCN2, 0.41 ± 0.18 μM ($n = 3$) for K452A, 0.52 ± 0.31 μM ($n = 3$) for R590A, and 350.3 ± 8.6 μM ($n = 3$) for R591E.

from a different angle. Using fluorescent cAMP molecules as a marker for ligand binding, as well as the PCF technique, recent studies on the HCN2 channel have shown a significant increase in cAMP binding corresponding to channel activation (46–48). This observation provides direct support for the long-held notion that the ligand opens the channel by preferably binding to and stabilizing the channel in an open state (49). In contrast to classical electrophysiology techniques such as TEVC and patch-clamp recording, PCF enables the separation of channel opening and ligand binding, two critical factors analogous to substrate binding and enzyme catalysis that have been difficult to distinguish, and thus is indispensable for specifically detecting ligand binding in a certain functional state (50).

The dual regulation of HCN channels by both voltage and cAMP provides a great opportunity for studying state-dependent ligand binding. We used a single hyperpolarizing voltage step to activate the channel and collected a series of fluorescence images of membrane patch, with NBD-cAMP serving as a marker for binding (Fig. 6 *A*, Table S2, and Supporting Material). For the WT mHCN2 channel, we observed a significant increase in cAMP binding corresponding to channel opening (*black trace*, Fig. 6, *B* and *C*). For the K452A channel, the increase in cAMP binding corresponding to channel activation (ΔΔF) is comparable to that of the WT channel (Fig. 6, *C* and *D*). However, during channel deactivation, cAMP unbinding is significantly slower (independent *t*-test, $t = 2.86$, $p < 0.05$). This slow release of cAMP during channel deactivation may explain the enhanced response to cAMP observed in the K452A mutant channel. In contrast, the maximal ΔΔF in R590A mutant channel is significantly reduced ($t = 7.81$, $p < 0.01$). Thus, in agreement with the electrophysiological characterizations showing that K452A enhances and R590A decreases the response to cAMP, PCF experiments demonstrate correlated changes in the dynamic interactions between cAMP and the full-length channel. These results provide direct evidence that mutations affecting the allosteric coupling perturb the dynamic, state-dependent binding of cAMP to the full-length HCN channel.

DISCUSSION

A common feature that is shared by many signaling proteins under allosteric regulation is multimeric assembly (51). In voltage-gated and ligand-gated ion channels, the positive cooperativity among subunits within a functional channel greatly enhances the sensitivity to external stimuli. Conversely, the negative cooperativity expands the range of detection. Consistent with the functional evidence supporting the cooperativity among four subunits during cAMP-dependent gating, the CL-CLBD structure reveals an extensive network of intersubunit contacts (25,26). However, our understanding of the functions of intersubunit contacts has been limited, due in part to the difficulty of teasing out the critical interactions from a network of complicated interactions (31). In this study, we performed a systematic survey of intersubunit contacts using an NMA-based covariance analysis. Subsequent functional assays confirmed that these intersubunit contacts play

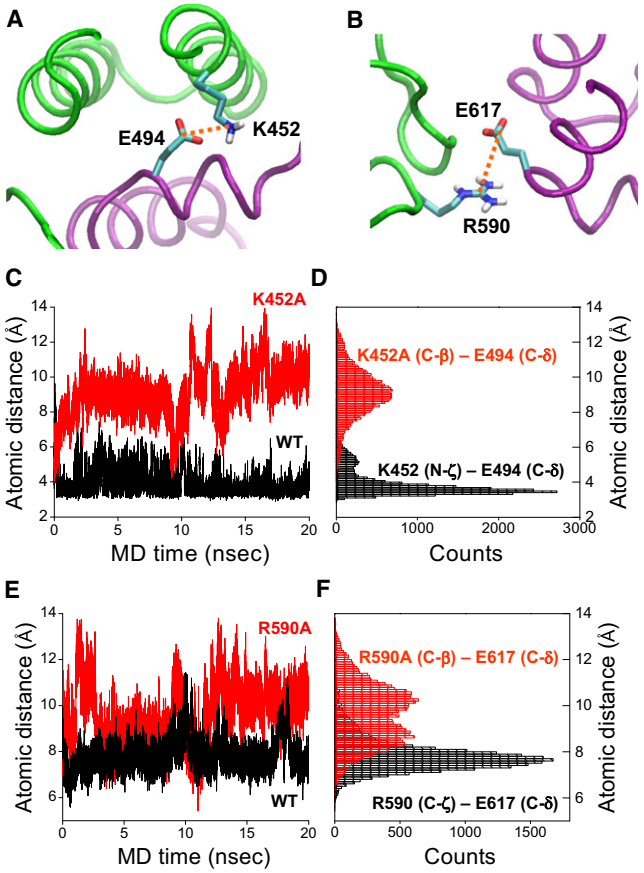

FIGURE 5 MD simulations reveal the disruption of electrostatic interactions involving K452A or R590A. (*A*) Close-up view of the interaction between K452 and E494. (*B*) View of the interaction between R590 and E617. (*C*) Atomic distances of K452 N-ζ-E494 C-δ atoms for WT protein or K452A C-β-E617 C-δ atoms for K452A proteins plotted as a function of MD simulation time. (*D*) Histogram of the atomic distances based on a 20-ns-long MD trajectory. (*E*) Distances of R590 C-ζ-E617 C-δ atoms for WT protein or R590A C-β-E617 C-ζ for R690A protein. (*F*) Histogram of the atomic distances based on a 20-ns-long MD trajectory.

a critical role in mediating the allosteric coupling between ligand binding and channel opening.

Studying interfacial contacts in a newly solved crystal structure has been established as a routine practice. Simply analyzing the structure is challenging because of the difficulty of identifying the critical components in a complicated network of interacting atoms and residues. Alternatively, analysis based on contact maps is an oversimplified approach, because interfacial contacts can be supported by long-range interactions involving residues that are not in direct contact (Fig. S2). As a result of dewetting of polar side chains at the interface, the local dielectric constant can be as low as in the interior of the protein, which directly promotes long-range electrostatic interactions. Hence, a systematic survey of all contacts should be very useful. Here, we began by using NMA, an analytical approach for protein dynamics based on a description of the system by potential energy functions. Another advantage of this method is the remarkable reduction in the degree-of-freedom from $3 \times N$, for a system containing N particles, to the number of collective motions that dominate the atomic fluctuations (16,52–56). We chose the first 100 modes for the AANMA and the first five for the ANM-based NMA, both of which are significantly smaller than the degree-of-freedom of the whole system (AANMA: 64,599; ANM: 2400). The accuracy and effectiveness of this NMA-based covariance analysis were confirmed by the successful delineation of the essential cAMP-CNBD contacts as well as the reproduction of secondary structure skeletons. Moreover, to further verify the robustness of this approach, we tested the NMA based on ANM, which considers only C-α atoms, and obtained results that are highly comparable to the AANMA results. Because the ANM model ignores the detailed chemical information embedded in the structure, our results support the notion that the shape of the protein molecule critically determines the dynamics and function of the protein (36). In recent years, other computational methods have been developed to predict allosteric pathways, including the Markovian propagation of signals approach, which is also based on the ANM (57,58).

In addition to NMA, another widely used computational approach for studying protein dynamics is the PCA, a statistical analysis based on MD or MC simulations. Both NMA and MD-based PCA can be traced to the definition of system potential energy, but they are significantly different. NMA focuses on the dynamic behavior of a protein molecule within a harmonic energy well, which is most likely where the original crystal structure stays. However, the MD-based PCA is a statistical approach based on a sampling of protein conformation space by an MD simulation. In most MD simulations, the propagation of conformation sampling is random. Our preliminary results show that the MD-PCA method can successfully reproduce the local cAMP-CNBD contacts as well as the secondary structural elements within the same subunit, but the results for the intersubunit contacts are not consistent. Still, the MD-based PCA has great potential because the MD simulation has the advantage of incorporating factors such as solvent and temperature, and can more faithfully reproduce the dynamic behavior of protein molecules under native conditions (59–62). Further investigation will be needed to exploit the full potential of MD-based PCA for delineating crucial atomic contacts.

To test the predicted critical atomic contacts experimentally, we mutated the residues to alanine and employed a multidisciplinary approach to characterize the mutant channels. Electrophysiological recordings provide a seamless view of ionic flow through the open channel but very limited information regarding two important issues: ligand binding and channel gating (50). On the other hand, biochemical binding assays on isolated CL-CNBD protein yield information about local contacts between cAMP and

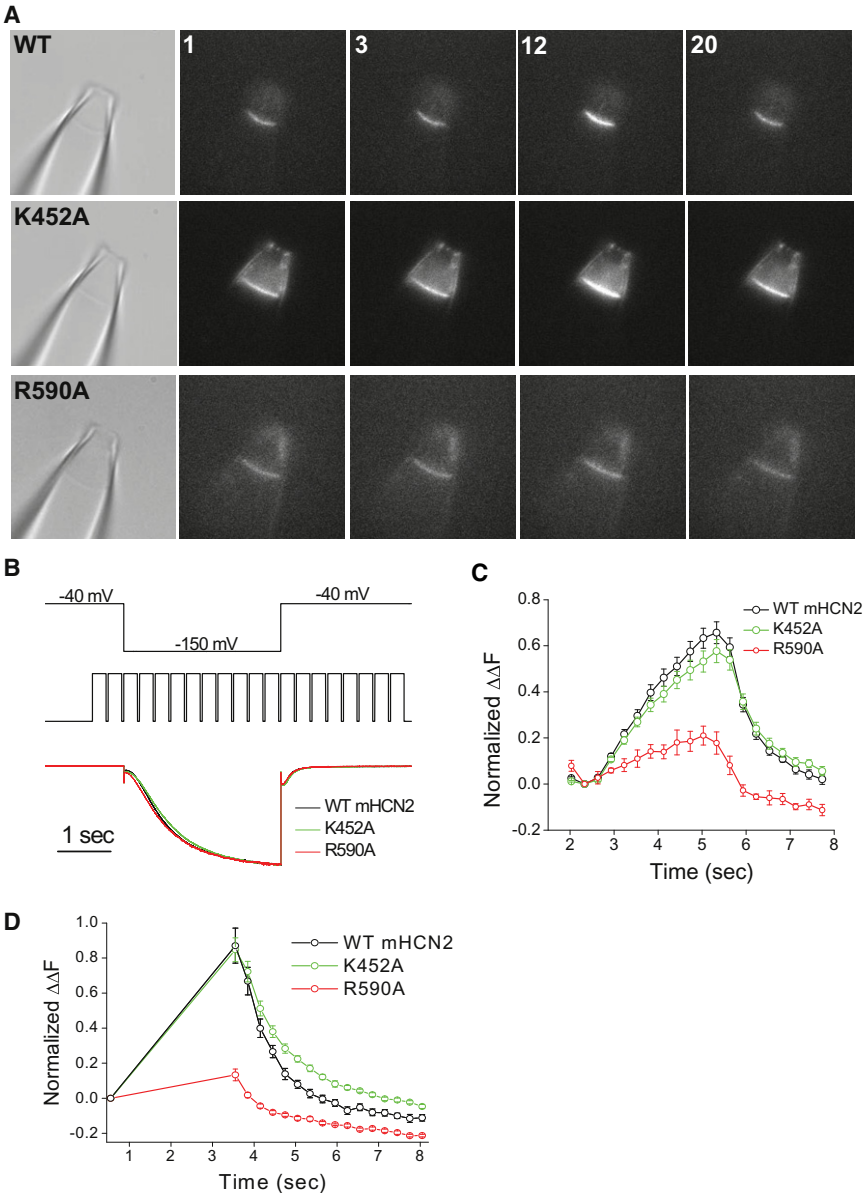

FIGURE 6 PCF measurements of full-length K452A and R590A mutant channels. (*A*) Bright-field images showing excised membrane patches (*left*) and fluorescence images collected along the voltage step. The timing of image collection is shown in *B*. (*B*) Top: Hyperpolarizing voltage step used for channel activation. Middle: TTL signal from the CCD camera exposure port showing the timing of image collection. Bottom: Normalized macroscopic current traces. (*C*) Fluorescence signal normalized to the intensity measured at −40 mV. A 20-image protocol as shown in *B* was used to record the dynamic cAMP binding during channel activation and deactivation. (*D*) A 17-image protocol was used to specifically detect the decay of fluorescence intensity during channel deactivation. Notice the increase in the release time constant for the K452A channel and the decrease in dynamic cAMP binding (ΔΔF) for the R590A channel compared with the WT channel.

CNBD, but reveal little about the allosteric coupling between cAMP binding and channel opening. The two mutations we focused on, K452A and R590A, significantly altered the response to cAMP in the whole channel but had minimal effects on the local interaction between cAMP and the isolated CL+CNBD fragment. Therefore, in agreement with the spatial localization of both residues (distant from either the CNBD or the channel gate), these results highlight the need to investigate cAMP-whole channel interactions. Indeed, the PCF assay convincingly shows that K452A slows down the release of cAMP during channel deactivation, whereas R590A reduces the activity-dependent increase in cAMP binding upon channel activation. In conjunction with electrophysiology recordings and biochemical binding assays, these studies provide a greater understanding of the intersubunit contacts at both local and global levels, and further reinforce the notion that the dynamic interaction between ligand and whole protein is crucial in ligand gating. To pinpoint the mechanism of allosteric coupling at the atomic level, it will be necessary to compare the full-length channel structures with or without cAMP. It is very possible that major structural differences reside in the subunit assembly and involve the crucial intersubunit contacts identified in this work.

To look further into the atomic details of those intersubunit contacts, we investigated the electrostatic interactions between K452 and its surrounding residues. We mutated the K452 residue to a negatively charged glutamate (K452E). As evidenced by TEVC experiments, K452E abolishes the response to cAMP and makes the channel behave in the

same manner as the R591E channel, which supports the importance of the electrostatic interaction between K452 and its neighboring residues (Fig. S4). We then looked at the nearby negatively charged residues to determine whether the phenotype of K452E could be rescued by charge swapping. Indeed, the channel containing the double mutations, K452E + E494R, causes the channel to behave similarly to the WT channel. However, the channel containing only the E494R mutation behaves normally, which is puzzling because presumably it should disrupt the electrostatic interaction with K452 and E494. It is possible that complicated structural rearrangements occur upon introduction of the E494R mutation. As a result, K452 comes into contact with other residues instead. It is recognized that a single point mutation can introduce not only local but also global structural perturbations, complicating the interpretation of mutagenesis results.

In summary, in this work we combined computational and experimental approaches to systematically study the critical intersubunit contacts in cAMP-dependent gating in the HCN channel. We identified residues that are located a great distance away from the ligand-binding site but nevertheless are critical for the gating process. These intersubunit contacts not only function as a molecular scaffold but also play critical roles in allosteric coupling, which at the molecular level is implemented through the dynamic, state-dependent interaction between ligand and the whole channel. This strategy of teasing out critical atomic contacts based on covariance analysis potentially could be applied to other types of proteins under allosteric regulation.

SUPPORTING MATERIAL

Supplemental methods, four figures, two tables, and references (63–68) are available at http://www.biophysj.org/biophysj/supplemental/S0006-3495(12)00583-8.

We thank Drs. S. Siegelbaum and J. Hackett for their support and comments on this study, and H. Vaananen and S. Gruszecki for technical support.

This work was supported by the Virginia Commonwealth University Startup Fund and the American Heart Association (grant-in-aid to L.Z. and Q.L.), and a New Scholar Award in Aging from the Ellison Medical Foundation to Q.L.

REFERENCES

1. Sakmann, B., and E. Neher. 1984. Patch clamp techniques for studying ionic channels in excitable membranes. *Annu. Rev. Physiol.* 46: 455–472.
2. Sigworth, F. J. 1986. The patch clamp is more useful than anyone had expected. *Fed. Proc.* 45:2673–2677.
3. Stevens, C. F. 1984. Biophysical studies of ion channels. *Science.* 225:1346–1350.
4. Tsai, C. J., A. Del Sol, and R. Nussinov. 2009. Protein allostery, signal transmission and dynamics: a classification scheme of allosteric mechanisms. *Mol. Biosyst.* 5:207–216.
5. Hammes-Schiffer, S., and S. J. Benkovic. 2006. Relating protein motion to catalysis. *Annu. Rev. Biochem.* 75:519–541.
6. Henzler-Wildman, K. A., V. Thai, …, D. Kern. 2007. Intrinsic motions along an enzymatic reaction trajectory. *Nature.* 450:838–844.
7. Henzler-Wildman, K. A., M. Lei, …, D. Kern. 2007. A hierarchy of timescales in protein dynamics is linked to enzyme catalysis. *Nature.* 450:913–916.
8. Eisenmesser, E. Z., O. Millet, …, D. Kern. 2005. Intrinsic dynamics of an enzyme underlies catalysis. *Nature.* 438:117–121.
9. Van Wynsberghe, A. W., and Q. Cui. 2006. Interpreting correlated motions using normal mode analysis. *Structure.* 14:1647–1653.
10. Go, N. 1990. A theorem on amplitudes of thermal atomic fluctuations in large molecules assuming specific conformations calculated by normal mode analysis. *Biophys. Chem.* 35:105–112.
11. Berendsen, H. J., and S. Hayward. 2000. Collective protein dynamics in relation to function. *Curr. Opin. Struct. Biol.* 10:165–169.
12. Kitao, A., and N. Go. 1999. Investigating protein dynamics in collective coordinate space. *Curr. Opin. Struct. Biol.* 9:164–169.
13. Brooks, B. R., D. Janezic, and M. Karplus. 1995. Harmonic analysis of large systems. I. Methodology. *J. Comput. Chem.* 16:1522–1542.
14. Amadei, A., A. B. Linssen, and H. J. Berendsen. 1993. Essential dynamics of proteins. *Proteins.* 17:412–425.
15. Ma, J. 2005. Usefulness and limitations of normal mode analysis in modeling dynamics of biomolecular complexes. *Structure.* 13:373–380.
16. Ichiye, T., and M. Karplus. 1991. Collective motions in proteins: a covariance analysis of atomic fluctuations in molecular dynamics and normal mode simulations. *Proteins.* 11:205–217.
17. Bell, D. C., H. Yao, …, S. A. Siegelbaum. 2004. Changes in local S4 environment provide a voltage-sensing mechanism for mammalian hyperpolarization-activated HCN channels. *J. Gen. Physiol.* 123:5–19.
18. Männikkö, R., F. Elinder, and H. P. Larsson. 2002. Voltage-sensing mechanism is conserved among ion channels gated by opposite voltages. *Nature.* 419:837–841.
19. Craven, K. B., and W. N. Zagotta. 2006. CNG and HCN channels: two peas, one pod. *Annu. Rev. Physiol.* 68:375–401.
20. Biel, M. 2009. Cyclic nucleotide-regulated cation channels. *J. Biol. Chem.* 284:9017–9021.
21. Zagotta, W. N., and S. A. Siegelbaum. 1996. Structure and function of cyclic nucleotide-gated channels. *Annu. Rev. Neurosci.* 19:235–263.
22. Berman, H. M., L. F. Ten Eyck, …, S. S. Taylor. 2005. The cAMP binding domain: an ancient signaling module. *Proc. Natl. Acad. Sci. USA.* 102:45–50.
23. Zagotta, W. N., N. B. Olivier, …, E. Gouaux. 2003. Structural basis for modulation and agonist specificity of HCN pacemaker channels. *Nature.* 425:200–205.
24. Xu, X., Z. V. Vysotskaya, …, L. Zhou. 2010. Structural basis for the cAMP-dependent gating in the human HCN4 channel. *J. Biol. Chem.* 285:37082–37091.
25. Ulens, C., and S. A. Siegelbaum. 2003. Regulation of hyperpolarization-activated HCN channels by cAMP through a gating switch in binding domain symmetry. *Neuron.* 40:959–970.
26. Altomare, C., A. Bucchi, …, D. DiFrancesco. 2001. Integrated allosteric model of voltage gating of HCN channels. *J. Gen. Physiol.* 117:519–532.
27. Kusch, J., S. Thon, …, K. Benndorf. 2012. How subunits cooperate in cAMP-induced activation of homotetrameric HCN2 channels. *Nat. Chem. Biol.* 8:162–169.
28. Kaupp, U. B., and R. Seifert. 2002. Cyclic nucleotide-gated ion channels. *Physiol. Rev.* 82:769–824.
29. Gavazzo, P., C. Picco, …, A. Menini. 2000. A point mutation in the pore region alters gating, Ca(2+) blockage, and permeation of olfactory cyclic nucleotide-gated channels. *J. Gen. Physiol.* 116:311–326.
30. Varnum, M. D., and W. N. Zagotta. 1997. Interdomain interactions underlying activation of cyclic nucleotide-gated channels. *Science.* 278:110–113.

31. Craven, K. B., and W. N. Zagotta. 2004. Salt bridges and gating in the COOH-terminal region of HCN2 and CNGA1 channels. *J. Gen. Physiol.* 124:663–677.

32. Hamelberg, D., T. Shen, and J. A. McCammon. 2006. Insight into the role of hydration on protein dynamics. *J. Chem. Phys.* 125:094905.

33. Moritsugu, K., and J. C. Smith. 2005. Langevin model of the temperature and hydration dependence of protein vibrational dynamics. *J. Phys. Chem. B.* 109:12182–12194.

34. Bahar, I., A. R. Atilgan, and B. Erman. 1997. Direct evaluation of thermal fluctuations in proteins using a single-parameter harmonic potential. *Fold. Des.* 2:173–181.

35. Yang, L. W., E. Eyal, …, I. Bahar. 2007. Insights into equilibrium dynamics of proteins from comparison of NMR and X-ray data with computational predictions. *Structure.* 15:741–749.

36. Tama, F., and C. L. Brooks. 2006. Symmetry, form, and shape: guiding principles for robustness in macromolecular machines. *Annu. Rev. Biophys. Biomol. Struct.* 35:115–133.

37. Zhou, L., and S. A. Siegelbaum. 2007. Gating of HCN channels by cyclic nucleotides: residue contacts that underlie ligand binding, selectivity, and efficacy. *Structure.* 15:655–670.

38. Seifert, R., A. Scholten, …, U. B. Kaupp. 1999. Molecular characterization of a slowly gating human hyperpolarization-activated channel predominantly expressed in thalamus, heart, and testis. *Proc. Natl. Acad. Sci. USA.* 96:9391–9396.

39. Santoro, B., S. Chen, …, S. A. Siegelbaum. 2000. Molecular and functional heterogeneity of hyperpolarization-activated pacemaker channels in the mouse CNS. *J. Neurosci.* 20:5264–5275.

40. Wang, J., S. Chen, …, S. A. Siegelbaum. 2002. Activity-dependent regulation of HCN pacemaker channels by cyclic AMP: signaling through dynamic allosteric coupling. *Neuron.* 36:451–461.

41. Chen, S., J. Wang, and S. A. Siegelbaum. 2001. Properties of hyperpolarization-activated pacemaker current defined by coassembly of HCN1 and HCN2 subunits and basal modulation by cyclic nucleotide. *J. Gen. Physiol.* 117:491–504.

42. Reference deleted in proof.

43. Roux, B., and K. Schulten. 2004. Computational studies of membrane channels. *Structure.* 12:1343–1351.

44. Stansfeld, P. J., and M. S. Sansom. 2011. Molecular simulation approaches to membrane proteins. *Structure.* 19:1562–1572.

45. Karplus, M., and J. A. McCammon. 2002. Molecular dynamics simulations of biomolecules. *Nat. Struct. Biol.* 9:646–652.

46. Wu, S., Z. V. Vysotskaya, …, L. Zhou. 2011. State-dependent cAMP binding to functioning HCN channels studied by patch-clamp fluorometry. *Biophys. J.* 100:1226–1232.

47. Kusch, J., C. Biskup, …, K. Benndorf. 2010. Interdependence of receptor activation and ligand binding in HCN2 pacemaker channels. *Neuron.* 67:75–85.

48. Biskup, C., J. Kusch, …, K. Benndorf. 2007. Relating ligand binding to activation gating in CNGA2 channels. *Nature.* 446:440–443.

49. Goh, C. S., D. Milburn, and M. Gerstein. 2004. Conformational changes associated with protein-protein interactions. *Curr. Opin. Struct. Biol.* 14:104–109.

50. Colquhoun, D. 1998. Binding, gating, affinity and efficacy: the interpretation of structure-activity relationships for agonists and of the effects of mutating receptors. *Br. J. Pharmacol.* 125:924–947.

51. Changeux, J. P., and S. J. Edelstein. 2005. Allosteric mechanisms of signal transduction. *Science.* 308:1424–1428.

52. Suhre, K., and Y. H. Sanejouand. 2004. On the potential of normal-mode analysis for solving difficult molecular-replacement problems. *Acta Crystallogr. D Biol. Crystallogr.* 60:796–799.

53. Chen, X., B. K. Poon, …, J. Ma. 2007. Normal-mode refinement of anisotropic thermal parameters for potassium channel KcsA at 3.2 A crystallographic resolution. *Structure.* 15:955–962.

54. Bahar, I., T. R. Lezon, …, I. H. Shrivastava. 2010. Normal mode analysis of biomolecular structures: functional mechanisms of membrane proteins. *Chem. Rev.* 110:1463–1497.

55. Petrone, P., and V. S. Pande. 2006. Can conformational change be described by only a few normal modes? *Biophys. J.* 90:1583–1593.

56. Cui, Q., G. Li, …, M. Karplus. 2004. A normal mode analysis of structural plasticity in the biomolecular motor F(1)-ATPase. *J. Mol. Biol.* 340:345–372.

57. Tang, S., J. C. Liao, …, J. P. Schmidt. 2007. Predicting allosteric communication in myosin via a pathway of conserved residues. *J. Mol. Biol.* 373:1361–1373.

58. Chennubhotla, C., Z. Yang, and I. Bahar. 2008. Coupling between global dynamics and signal transduction pathways: a mechanism of allostery for chaperonin GroEL. *Mol. Biosyst.* 4:287–292.

59. Hess, B. 2000. Similarities between principal components of protein dynamics and random diffusion. *Phys. Rev. E.* 62(6 Pt. B):8438–8448.

60. Rueda, M., P. Chacón, and M. Orozco. 2007. Thorough validation of protein normal mode analysis: a comparative study with essential dynamics. *Structure.* 15:565–575.

61. Balsera, M. A., W. Wriggers, …, K. Schulten. 1996. Principal component analysis and long time protein dynamics. *J. Phys. Chem.* 100:2567–2572.

62. Amadei, A., B. L. de Groot, …, H. J. Berendsen. 1999. A kinetic model for the internal motions of proteins: diffusion between multiple harmonic wells. *Proteins.* 35:283–292.

63. Sali, A., L. Potterton, …, M. Karplus. 1995. Evaluation of comparative protein modeling by MODELLER. *Proteins.* 23:318–326.

64. Lindahl, E., B. Hess, and D. van der Spoel. 2001. GROMACS 3.0: a package for molecular simulation and trajectory analysis. *J. Mol. Model.* 7:306–317.

65. Schüttelkopf, A. W., and D. M. van Aalten. 2004. PRODRG: a tool for high-throughput crystallography of protein-ligand complexes. *Acta Crystallogr. D Biol. Crystallogr.* 60:1355–1363.

66. Zhou, L., and S. A. Siegelbaum. 2008. Effects of surface water on protein dynamics studied by a novel coarse-grained normal mode approach. *Biophys. J.* 94:3461–3474.

67. van der Spoel, D., and P. J. van Maaren. 2006. The origin of layer structure artifacts in simulations of liquid water. *J. Chem. Theory Comput.* 2:1–11.

68. Atilgan, A. R., S. R. Durell, …, I. Bahar. 2001. Anisotropy of fluctuation dynamics of proteins with an elastic network model. *Biophys. J.* 80:505–515.